Ocean Engineering 38 (2011) 673–683

Contents lists available at ScienceDirect

Ocean Engineering

journal homepage: www.elsevier.com/locate/oceaneng

Computational study on near wake interaction between undulation body and a D-section cylinder

Qing Xiao [a,*], Ke Sun [b], Hao Liu [c], Jianxin Hu [a]

[a] Department of Naval Architecture and Marine Engineering, University of Strathclyde, Glasgow G4 0LZ, UK
[b] College of Shipbuilding Engineering, Harbin Engineering University, Harbin 150001, PR China
[c] Department of Biomechanical Engineering, Chiba University, Chiba 263-8522, Japan

ARTICLE INFO

Article history:
Received 15 September 2010
Accepted 27 December 2010
Editor-in-Chief: A.I. Incecik
Available online 22 January 2011

Keywords:
Undulation foil
Cylinder drag reduction
Thrust generation
Vortex control

ABSTRACT

We present a numerical study on the hydrodynamic performance of undulation NACA0012 foil in the near wake of D-section cylinder. Computations are conducted using unsteady incompressible Navier–Stokes equations with a moving adaptive mesh based on laminar flow. Investigations are focused on the effect of distance ratio between foil tip and centre of cylinder ($L/D \leq 2.0$) on the thrust/drag performance of foil and cylinder at various foil undulation frequency (St). We found that, foil thrust coefficient (C_t) increases considerably with the appearance of cylinder and an optimal distance exists at which C_t reaches maxima. The maximum increment is about eleven times that of its counterpart of single foil, which is obtained at $St=0.23$ and $L/D=0.5$. Our results for the cylinder drag coefficient (C_d) observed the existence of optimal parametric map, combined with various gap ratios and foil frequencies. With these parameters, insertion of an undulation foil can significantly lead to the drag reduction indicating that undulating foil could work efficiently as a passive vortex control device for cylinder drag reduction.

1. Introduction

It is well known that fish prefers to inhabit behind a refuge by taking advantage of low-pressure region combined with the vortex field in the wake of a bluff body to reduce the cost of its locomotion through exploiting the energy from oncoming vortices (Breder, 1965; Weihs, 1973; Webb, 1998; Herskin and Steffensen, 1998; Hinch and Rand, 2000). Typical examples include the fish swimming in schooling and river/ocean environments.

The fundamental hydrodynamic mechanism behind these phenomena is the vortex control through the interaction between the fish motion and oncoming vortices. Compared to the study on fish swimming in steady stream, the investigations on how fish hydrodynamic performance responses to the incoming vortices are relatively new and challenging, due to the complicated structure of the flow and its inherent strong unsteadiness. To simplify the problem, a stationary or oscillating cylinder is usually adopted as the most controllable vortex generator. Investigations on the biotic/abiotic fish behaviour including its kinematic locomotion, thrust and turning performance in the wake of cylinder are performed (Gopalkrishnan et al., 1994; Streitline et al., 1996; Liao et al., 2003a, 2003b, 2004; Beal et al., 2006; Liao, 2007; Eldredge and Pisani, 2008). Typical biotic fish includes the live/dead fish with active body locomotion, while abiotic fish is represented by a rigid stationary or flapping foil and their kinematic motions are either prescribed or activated as a result of interaction between their body movements and surrounding fluid.

Gopalkrishnan et al. (1994) studied the hydrodynamic performance of a heaving and pitching NACA0012 foil downstream of a heaving D-sectional cylinder. Experiments were performed with various foil pitching amplitudes, oscillation frequency and different separation distances (L/D) between foil and cylinder with $L/D > 3.5$ (where L is the distance between foil and cylinder centre and D is the diameter of cylinder). Three distinct stable wake structures were identified based on the flow visualisation results at $Re=500$, i.e. expanding wake, destructive interaction wake and constructive interaction wake. The Reynolds number is defined as $Re=U_\infty c/v$ with U_∞ being the free-stream velocity, c is the chord length of foil and v is the dynamic viscosity. Force measurement at $Re=20{,}000$ showed that the foil thrust coefficient increases considerably compared to the foil alone case, and the extent to which depends significantly on the spacing. The limited results for cylinder drag coefficient revealed that drag force does not differ from that of without foil, and this is independent on the separation length.

A series of experimental work have been conducted by Liao et al. (2003a, 2003b, 2004) on the investigation of live rainbow

* Corresponding author.
E-mail addresses: qing.xiao@strath.ac.uk (Q. Xiao), sunke@hrbeu.edu.cn (K. Sun), hliu@faculty.chiba-u.jp (H. Liu), jianxin.hu@strath.ac.uk (J. Hu).

0029-8018/$ - see front matter © 2011 Elsevier Ltd. All rights reserved.
doi:10.1016/j.oceaneng.2010.12.017

trout in response to the hydrodynamic wake change of D-sectional cylinder. By measuring the fish body's kinematics like body amplitude, maximum curvature and tail-beat frequency, they observed that fish could synchronise their body kinematics to the vortices shedding from cylinder through extraction energy from vortices and thus use reduced muscle activity to retain their stationary positions or propel them upstream. The variation of cylinder vortices is achieved by altering the cylinder diameter or incoming free-stream velocity.

Beal et al. (2006) studied two cases for the interaction between D cylinder and downstream fish system, e.g. a stationary cylinder with a dead fish and a heaving cylinder with a passively mounted high-aspect-ratio flapping NACA0012 foil. Their experimental results for dead fish on its mid-line motion revealed the forward motion of fish from 4.0 to 1.75 D. For passively mounted foil, the pitching and heaving displacement were measured and their results proved that the positive thrust can be created by capturing vortices energy under proper conditions.

Recently, the behaviour of a fish-like system consisting of free or locked hinge-linked rigid body in the wake of a circular cylinder was studied computationally by Eldredge and Pisani (2008) at $Re=100$. Similar to Beal et al.'s experimental results, they found that, for certain ratio of body length to cylinder diameter, the fish placed three times the cylinder diameter downstream, presents a passively propelled motion toward the cylinder.

Interesting to note that, most of the above studies on the interference between cylinder and fish are concentrated on the hydrodynamics of the fish, rather than the front cylinder. However, it is apparent that such interaction has definite impact on the hydrodynamic performance of the cylinder depending on the motion of the fish, the size of the fish compared to the cylinder, the spacing between fish and cylinder and the Reynolds number as well.

The vortex shedding control, either actively or passively, to reduce the drag force of cylinder is a classic research topic due to its extensive applications in engineering. One of the efficient passive control methods proposed by previous researchers is using vortex splitter device. (See review papers of Zdravkovich (1981) and Choi et al. (2008)) Some examples include the attached or detached split plate (Kwon and Choi, 1996; Hwang et al., 2003), small control cylinders (Strykowski and Sreenivasan, 1990) and stationary foil (Liao et al., 2004). It is generally accepted that by applying this technique, the structure of the classic Karman vortex street in the wake of cylinder is altered and the resulted drag force can be increased or decreased, relying on the size of split device and the gap between cylinder and device.

In this paper, the study on the interaction between an undulation NACA0012 foil in the wake of a D-section cylinder is numerically performed. Different from previous investigations, attention will be focused not only on foil hydrodynamic performance, but also on that of the cylinder. Although the concept of using insertion in the wake of cylinder to reduce drag force is not new, most of previous insertions are the stationary plate or foil. Little work has been done with oscillating foil, especially the kinematic motion based on the undulation locomotion, which is closer to the cannigform fish swimming. The conclusions drawn from this study therefore, will be significant for the research on the locomotion rules of large-scale fish and their interaction with habitats, the propulsive device design and vortex shedding control in the wake of cylinder. Moreover, the foil in previous studies is exclusively placed behind the cylinder beyond a distance 2.5 the diameter of cylinder, which is generally known as 'suction region'. It is believed that, the detailed physics of vortex development in the near wake ($L/D \leq 2.0$) and its effect on the thrust /drag performance of foil/cylinder, could be different from that of further apart foil cylinder system.

The rest of the paper is organised in the following manner. We begin by outlining the computational approach in Section 2 including the numerical methods, kinematic model of undulation fish and some relevant problem description parameters. In Section 3, computational results for flows involving a single D cylinder, single fish and combined fish and cylinder are presented and discussed along with the in-depth analysis on the flow phenomena. This is followed by the concluding remarks.

2. Computational approach

2.1. Problem description

In this study, the flow over an NACA0012 undulation foil in the near wake of D cylinder is modelled and the interaction between two objects is studied. The flow configuration is shown in Fig. 1. The foil with chord length of c is arranged along the centreline of D-section cylinder, and the gap between foil tip to cylinder centre L is adjustable. Key non-dimensional parameters include the gap ratio based on the cylinder diameter L/D and relative size of fish and cylinder D/c. Computations are conducted for five gap ratios ($L/D=\infty$, 0.5, 1.0, 1.5 and 2.0) and D/c of 1.0. Note that, $L/D=\infty$ represents the case for either a single foil or a single cylinder. The Reynolds number in this study is fixed as 4.5×10^4 in all computations.

The present kinematic motion of the undulation fish is taken from subcarangiform swimming mode particularly a rainbow trout and expressed in Eq. (1). Several previous numerical and experimental studies have been done focusing on the flow around a single fish without D cylinder, for example Liao et al. (2003b) and Flanagan (2004). In the present study, this kinematic model is adopted to modelling the centreline movement of an undulating NACA0012 foil. The instant lateral excursion $h(x,t)$is expressed as:

$$h(x,t)=a(x)\sin\left[2\pi\left(\frac{x}{\lambda}-\frac{t}{T}\right)\right] \tag{1}$$

where $a(x)$ represents the lateral wave amplitude, x is the lengthwise coordinate measured from the tip of the fish head (leading edge of foil), t is the instant time, λ is the wavelength and T is the undulation period. The amplitude $a(x)$ is expressed as a sinusoidal equation as follows:

$$a(x)=L\left[0.351\sin\left(\frac{x}{L}-1.796\right)+0.359\right] \tag{2}$$

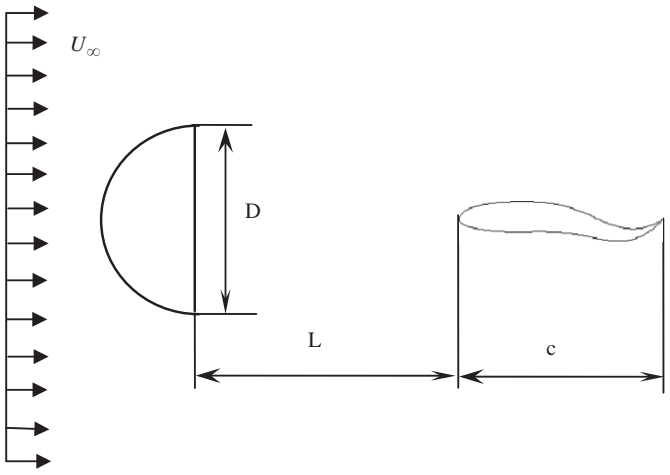

Fig. 1. Schematic of flow configuration.

In all our computations, the wavelength λ and amplitude $a(x)$ parameters are specified and fixed at $\lambda=0.115$ m. The baseline frequency (f) is taken from experimental work of Liao et al. (2003b). For a rainbow trout with a body length of 0.1 m, the wavelength λ is 0.115 m and the period T is 0.15 s, therefore the frequency f is 6.67 Hz and the ratio of wavelength to foil body length is 1.15. The non-dimensional oscillation frequency is defined by the Strouhal number as $St=fA/U_\infty$, where A is the foil tail amplitude. In this study, simulations are performed under different undulation frequency St varying from 0.12, 0.23, 1.18 to 1.76.

2.2. Numerical method

The flow is modelled by using commercial Computational Fluid Dynamics package FLUENT 6.3. The governing equations for the unsteady incompressible two-dimensional laminar flow are expressed as follows:

$$\nabla \cdot \mathbf{V} = 0 \tag{3}$$

$$\rho \frac{D\mathbf{V}}{Dt} = \mathbf{F} - \nabla p + \mu \nabla^2 \mathbf{V} \tag{4}$$

where $\mathbf{V}$ is the velocity vector, ρ is the density of the fluid, t is instant time, $\mathbf{F}$ is the body force acting on the fluid, p is the pressure, and μ is the dynamic viscosity of the fluid.

The governing Eqs. (3) and (4), are discretized using a finite volume method with an implicit first order time-marching scheme for unsteady term to allow time step being at a reasonable level. A second-order upwind scheme is used for convective terms and diffusion-term discretization is applied with the second-order central-differencing scheme. Pressure–velocity coupling of the continuity equation was achieved using the SIMPLE algorithm.

To capture the movement of foil in the computational domain, a dynamic grid scheme is used. There are three types of deforming mesh in FLUENT, i.e. smoothing method, dynamic layering and local regridding method. At each updated time instant, the foil centreline position is determined by Eq. (1) and the cells around the foil are regenerated and smoothed using FLUENT Macro GRID_MOTION function associated to regridding and smoothing methods. To ensure the grid quality at each time step, small time step sizes are required depending on the different undulation frequency with typical value of 500 in one particular time period.

2.3. Computational domain and boundary conditions

The computational domain and detailed grid distribution are illustrated in Fig. 2(a) and (b), respectively. Assuming foil chord length is c, the size of the computational domain is $16c \times 8c$, with the front tip of the fish located in the middle of the domain in the y-direction and $10.5c$ in the x-direction from the outflow boundary. An unstructured mesh is constructed within the area around the fish while for the rest of the computational domain, a structure mesh topology is adopted to minimise the computational time. To accurately capture the wake structure and surface force, the grid is distributed with higher resolutions near the body and in the wake of the foil. Grid dependence test is conducted for a medium grid (163520) and a fine grid (286984). Computational results for instant thrust coefficient are shown in Fig. 3 indicating no significant difference for the medium and fine grids and therefore medium grid is used for all computations. The average vertical distance of the first grid point apart from the foil wall is 10^{-3} chord length.

A uniform x-direction velocity is used as the inflow boundary condition, with $u=U_\infty$, $v=0$ and $\partial p/\partial x=0$. The outflow boundary condition is set as $\partial u/\partial x=0$, $\partial v/\partial x=0$ and $p=p_\infty$. Symmetry condition that effectively models the boundary as a slip wall is imposed on the upper and bottom computational domain. On the surface of the moving fish, velocity component in the x-direction u is equal to zero and v is determined by the kinematic Eq. (1).

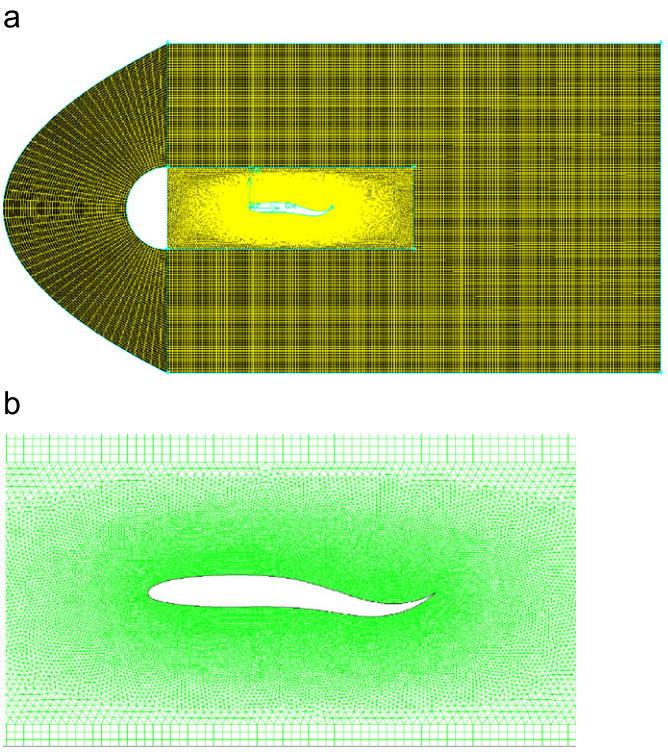

Fig. 2. Computational domain and grid display ($D/c=1.0$ and $L/c=1.0$): (a) global grid distribution and (b) grid distribution around foil.

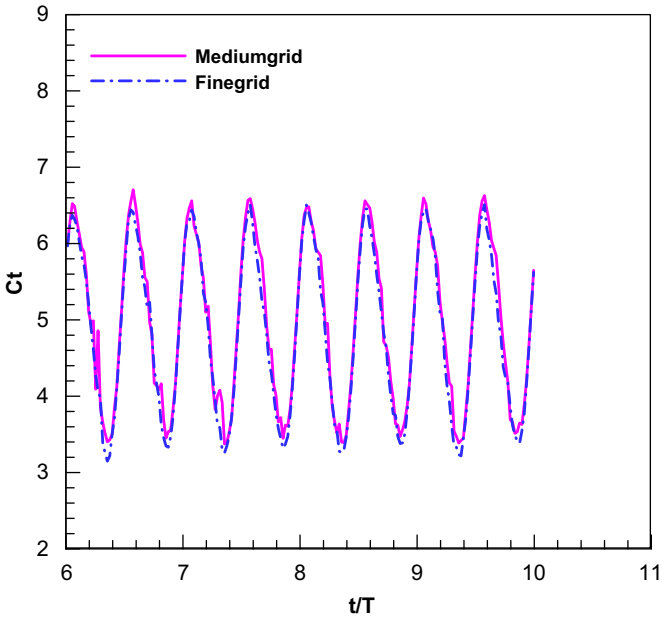

Fig. 3. Grid dependence test for undulation foil with $St=1.18$.

2.4. Force parameters

The foil thrust performance is quantified with the thrust force or thrust coefficient C_t. The overall force acting on the foil is composed of contributions from pressure and friction force. Assume that $\overline{F}_c$ is the time-averaged value of the force component

$X(t)$ on the foil in stream-wise direction and spanwise length of foil is 1.0, the thrust coefficient is defined as:

$$C_t = \frac{\overline{F_c}}{(1/2)\rho U_\infty^2 c} \tag{5}$$

Similarly, the drag coefficient of the cylinder C_d is determined by:

$$C_d = \frac{\overline{F_d}}{(1/2)\rho U_\infty^2 D} \tag{6}$$

where $\overline{F}_d$ is the time-averaged force component $X(t)$ of the cylinder in the stream-wise direction given by:

$$\overline{F_d} = \frac{1}{T}\int_0^T X(t)dt \tag{7}$$

where T is the time period.

The cylinder lift coefficient C_L is determined by:

$$C_L = \frac{\overline{F}_L}{(1/2)\rho U_\infty^2 D} \tag{8}$$

where $\overline{F}_L$ is the time-averaged force component $Y(t)$ of the cylinder in the vertical direction, determined by:

$$\overline{F}_L = \frac{1}{T}\int_0^T Y(t)dt \tag{9}$$

3. Results and discussions

3.1. Validation

To validate the numerical approach, two test cases are selected. The flow across a D-section cylinder is first considered. It is well known that beyond a threshold Reynolds number, vortex shedding downstream in the wake of a cylinder is an important feature of such flow. Here, the flow across the cylinder is simulated with an unsteady approach. The predicted non-dimensional vortex shedding frequency ($St = fD/U_\infty$) at different Reynolds number is compared with experimental results from Gopalkrishnan et al. (1994) as shown in Fig. 4. The computed results show a very good agreement with the experimental results exhibiting a good numerical capability for unsteady flow modelling.

The next step consists of the study of the flow over an undulation plate, which resembles the centreline, or backbone of a fish. The kinematic motion follows Eqs. (1) and (2) with the undulation period $T=0.15s$. The instantaneous velocity contours and vorticity contour around the plate at $t=7.0T$ are compared with numerical prediction by Flanagan (2004) as illustrated in Figs. 5 and 6. The predicted wake structure agrees very well with Flanagan's result revealing a reverse Karman vortex street with a downstream directed jet behind the plate. The alternating shedding vortices in the wake are evident in the contour plot of vorticity, as shown in Fig. 6. Positive vorticity (red centre) represents rotation in the counter-clockwise direction, while negative vorticity (blue centre) represents rotation in the clockwise direction.

3.2. Single D-section cylinder and single fish

Investigation on separated D cylinder and undulation NACA0012 foil is first conducted at Reynolds number of 4.5×10^4 as a reference for further studies on the combined D cylinder and foil case.

The typical instant cylinder drag/lift coefficient C_d and C_L variation with time are shown in Fig. 7(a) with unsteady solution approach at a time step of 0.01 s. As seen, C_d and C_L vary periodically with time after initial 300 iterations time, indicating the periodic vortex shedding in the wake of D cylinder at this Reynolds number. The time-mean lift coefficient presents a zero value while a positive drag coefficient of 2.06 is obtained. Considering the cylinder diameter of 0.1 m, the computed non-dimensional vortex shedding frequency St, by the Fast Fourier Transformation analysis, is 0.25.

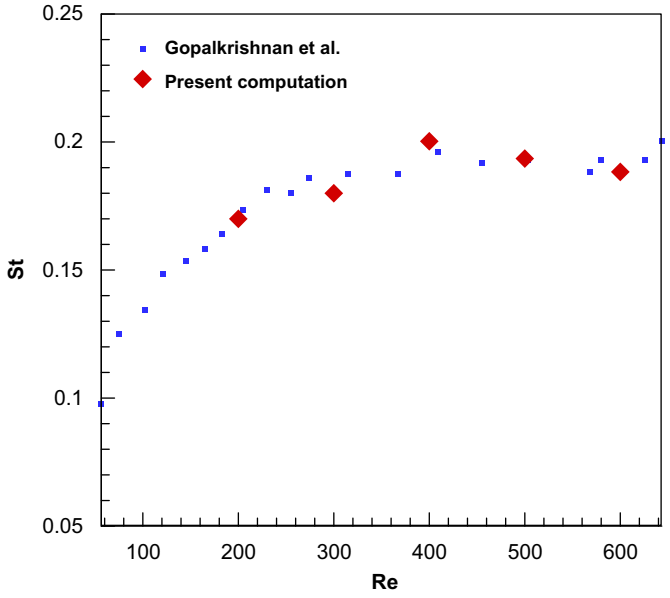

Fig. 4. Comparison of the Strouhal number vs. Reynolds number for D-section cylinder.

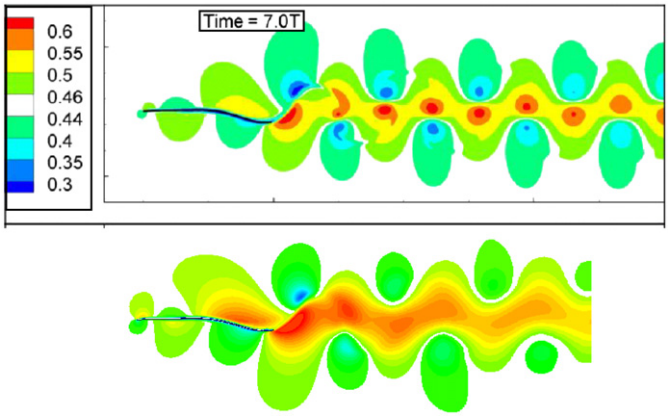

Fig. 5. Comparison between simulation by Flanagan (2004) (top) and present study (bottom) about the velocity contour (m/s) around a plate undergoing sinusoidal undulation motion.

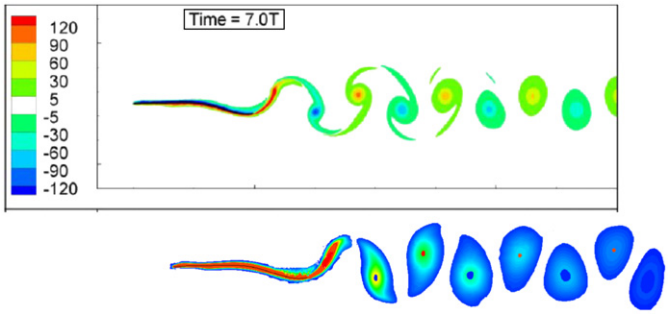

Fig. 6. Comparison between simulation by Flanagan (2004) (top) and present study (bottom) about the vorticity contour (1/s) around a plate undergoing sinusoidal undulation motion. (For interpretation of the references to colour in this figure, the reader is referred to the web version of this article.)

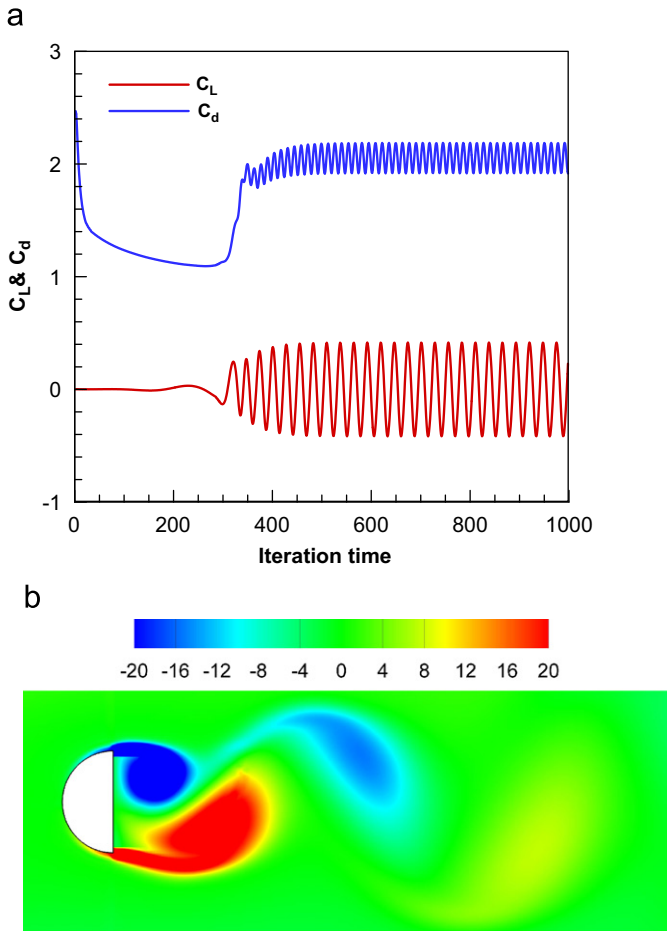

Fig. 7. (a) Variation of instant drag and lift coefficient of a single D cylinder with time and (b) instant vorticity contour in the wake of a D cylinder.

The vorticity contour is shown in Fig. 7(b), a classic Von Karman vortex street is clearly observed in the wake of cylinder up to 3.0D. Two rolls of vortexes appear with upper roll vortex rotates clockwise and bottom row rotates anti-clockwise.

Investigation on the single undulation foil is performed with various St from 0.12 to 1.76. The time-mean thrust coefficient increases with frequency as clearly seen in Fig. 8(a). At lowest frequency i.e. $St=0.12$, the locomotion of foil presents a drag-generated flow, while for the rest of frequency, positive thrust are observed. The time evolutions of instant thrust coefficient are shown in Fig. 8(b) for three frequencies. The increased amplitude and time-mean C_t is apparently revealed for high frequency. The corresponding vorticity contour in the downstream of foil at $St=1.18$ is shown in Fig. 8(c) at instant time of $1/5T$. Compared to Fig. 7(b) for the wake behind the cylinder, the vortex structure here displays a typical feature of the reserved Von Kaman street corresponding to the positive time-mean thrust generation.

As we can see from the above two separated cases, it would be expected that, if the foil is located in the near wake of the cylinder, the undulation of the foil will alter substantially the position and strength of the incoming cylinder vortices, thereby altering the hydrodynamics characteristics of the foil as well as the cylinder. The impact of such dependence is apparently associated with the gap ratio (L/D) and moreover the frequency of undulation foil.

3.3. Combined cylinder and fish effect on foil thrust

In this section, we present the computational results and discussions for combined D cylinder and fish, focusing on the thrust force variation with the insertion of a cylinder. We begin with how gap ratio affects the time-average thrust coefficient. In an effort to explain the mechanism of vortex shedding control, the vorticity contour and foil surface pressure distribution are compared for various cases with and without cylinder.

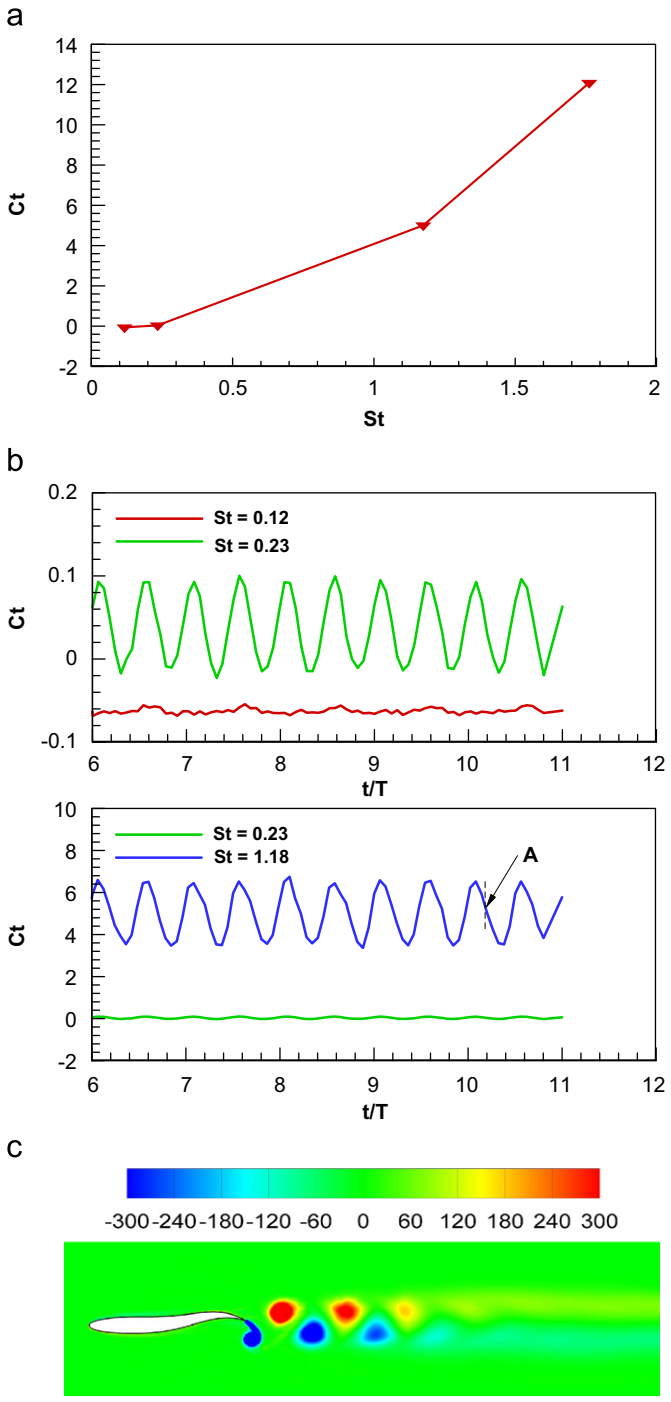

Fig. 8. (a) Time-mean thrust coefficient versus undulation frequency (Foil alone), (b) variation of instant thrust coefficient of undulation foil with time (Foil alone), and (c) vorticity contour in the wake of single undulation foil ($1/5T$ instant at $St=1.18$, A in Fig. 8(b)).

3.3.1. Time-mean thrust performance

Fig. 9(a) and (b) shows the time-average foil thrust coefficient (C_t) curve with different undulation frequency at various separation distance ($L/D=\infty$, 0.5, 1.0, 1.5, 2.0). Note that $L/D=\infty$

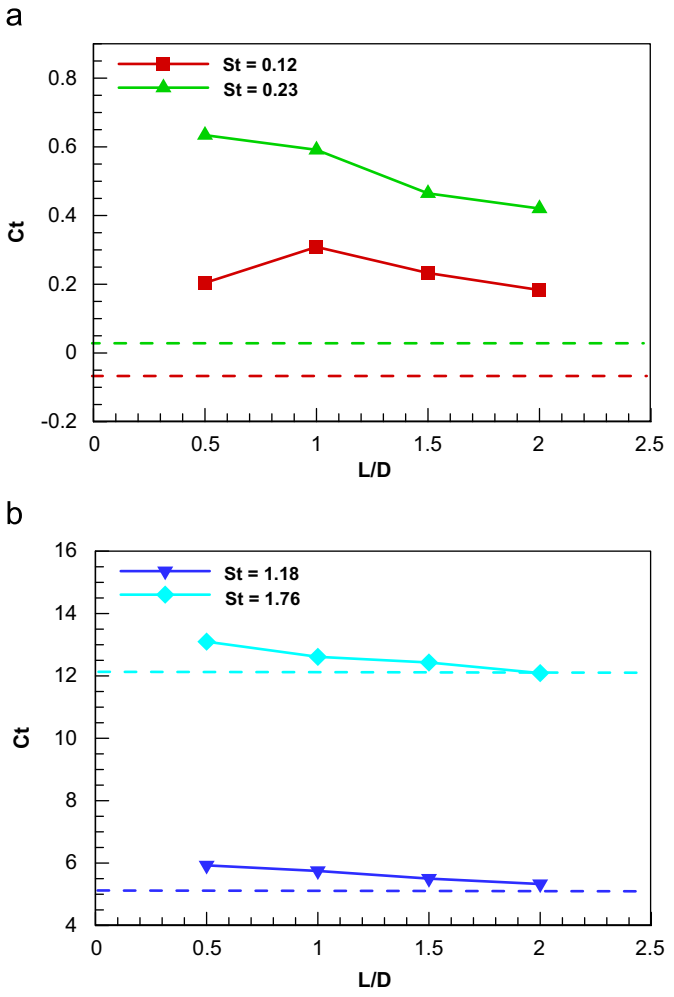

Fig. 9. The time-average thrust coefficient of foil with different undulation frequencies. (Combined foil and cylinder system). (a) $St=0.12$, 0.23 and (b) $St=1.18$, 1.76 (Dashed lines represent the corresponding data for single foil case).

represents the foil locomotion without cylinder. Clearly seen from Fig. 9, at the same L/D, C_t obtained by high frequency is always larger than that of low frequency indicating that larger thrust force could be obtained by increasing foil undulation frequency. This is true whether the foil undulates with or without a cylinder as displayed explicitly in Fig. 8(a) for single foil case.

The spacing effect of L/D on thrust coefficient displays common characteristics irrespective of the imposed frequency. The foil thrust, located in the wake of the cylinder, increases compared to that of single foil under the same frequency for all gap ratios tested. The increasing extent reduces with increased frequency. For example, at $St=0.23$ and $L/D=0.5$, C_t with a cylinder is about eleven times that of a single foil while for $St=1.76$ and $L/D=0.5$ this value drops to 1.1 times. Given a fixed frequency, an optimal gap ratio exists at which thrust coefficient reaches a maximum. For higher St (larger than 0.12), this gap ratio is 0.5 independent on the frequency. At $St=0.12$, an optimal gap ratio is observed at $L/D=1.0$.

3.3.2. Foil thrust enhancement mechanism

In this section, the mechanism of thrust enhancement at different frequency with various gap ratios is examined with the aid of computed vorticity contour, instant thrust evolution and foil surface pressure distribution are presented in Figs. 10–15.

The time history of instant thrust coefficient (C_t) with various gap ratios is shown in Figs. 10(a)–(e) and 11 for $St=0.12$ and 1.18, respectively. For high frequency as $St=1.18$, C_t versus time curve presents a periodic feature characterizing with one dominant frequency equal to imposed foil undulation frequency. As clearly revealed by the corresponding vorticity contours in Fig. 13 at $t/T=0$, three pairs of reversed Karman vortices are shedding in the foil wake for all spacing ratios investigated. The instant C_t for different L/D in Fig. 11 shows that, at $L/D=0.5$, foil oscillates at relative higher mean value indicating the optimal gap ratio of 0.5 at this frequency. Similar behaviour is obtained for $St=1.78$. With higher frequencies, it seems that the frequency of reversed Karman vortex shedding in the foil wake is not affected by the cylinder vortex shedding.

The situation changed at low frequencies like $St=0.12$. Depending on various gap ratios, C_t evolution with time shows either one or multiple oscillating frequencies. For the case without cylinder as plotted in Fig. 10(a), the foil C_t oscillates around a negative mean value. As seen in Fig. 12(a) for its counterpart vorticity contour, a classic Karman vortex street is observed in the foil wake, indicating a drag-producing situation. However, with the presence of a cylinder as shown in Fig. 10(b)–(e), the cylinder Karman vortex shedding behaviour is significantly altered (detailed discussion will be conducted later), which subsequently changes the vortex structure in the foil wake. Such behaviour is especially profound for low foil frequency and small gap ratios like $St=0.12$, $St=0.23$ and $L/D=0.5$–1.5. Recall that the Karman vortex shedding frequency for single D cylinder is $St=0.25$, which is very close to the imposed foil low frequency case. Under this circumstance, the interference between the foil and the cylinder is significant, which is reflected not only by the time-mean magnitude of C_t but also by the instant C_t, including the oscillating frequency as well as its amplitude. As seen in Fig. 10(b)–(d) for $L/D-0.5$ to 1.5, more than one dominant frequency is observed from C_t, curves along with the varied amplitude. Although the reversed Karman vortex is clearly seen from vorticity contours in Fig. 12(b)–(d), the multiple frequency features indicate that the vortex street is not fully developed. Except for the main reversed Karman vortices, some small vortices appear in the foil wake.

Further increasing the gap ratio to $L/D=2.0$, C_t curve shows periodic feature again and displays one dominated frequency which is about one third of the foil alone case. This indicates that, a fully developed cylinder vortex shedding is generated within such a relative large distance, and the interference between cylinder and foil reaches a stable condition resulting in a well developed reversed Kaman vortex street in the foil wake.

The vorticity contour in Fig. 12(c) clearly shows that at $L/D=1.0$, a pair of reversed Karman vortices are present in the foil wake with a very small separation region at the tip of the foil compared to the relative large leading edge separation at $L/D=1.5$ and 2.0. The optimal gap ratio at this frequency is therefore 1.0.

As we mentioned earlier, the total force on the foil consists of viscous force and pressure force. Our computation reveals that the viscous force represents only a minor percentage in the overall force, therefore, the force analysis is based on the pressure data. The surface pressure distributions along the top and bottom walls at $1/5T$ instant for $St=0.12$ and 1.18 are presented in Figs. 14 and 15, respectively. Similar trend is found for other time instants during one oscillating cycle. The pressure coefficient C_p is defined as:

$$C_p = \frac{p-p_\infty}{(1/2)\rho U_\infty^2 c} \tag{10}$$

where p_∞ is the ambient pressure.

The pressure distributions display a distinct difference between low and high foil frequency. With low frequencies like $St=0.12$ in Fig. 14, the pressure variation along the surface is not significant which is especially true at the foil bottom wall for all gap ratios. Similar trend is also present on the foil top surface for $L/D<2.0$. At $L/D=2.0$, a pressure dip on the top wall is observed at around $x/c=0.85$ caused by the vortex generated on the top surface as seen from vorticity contour in Fig. 12(e). For high frequencies such as

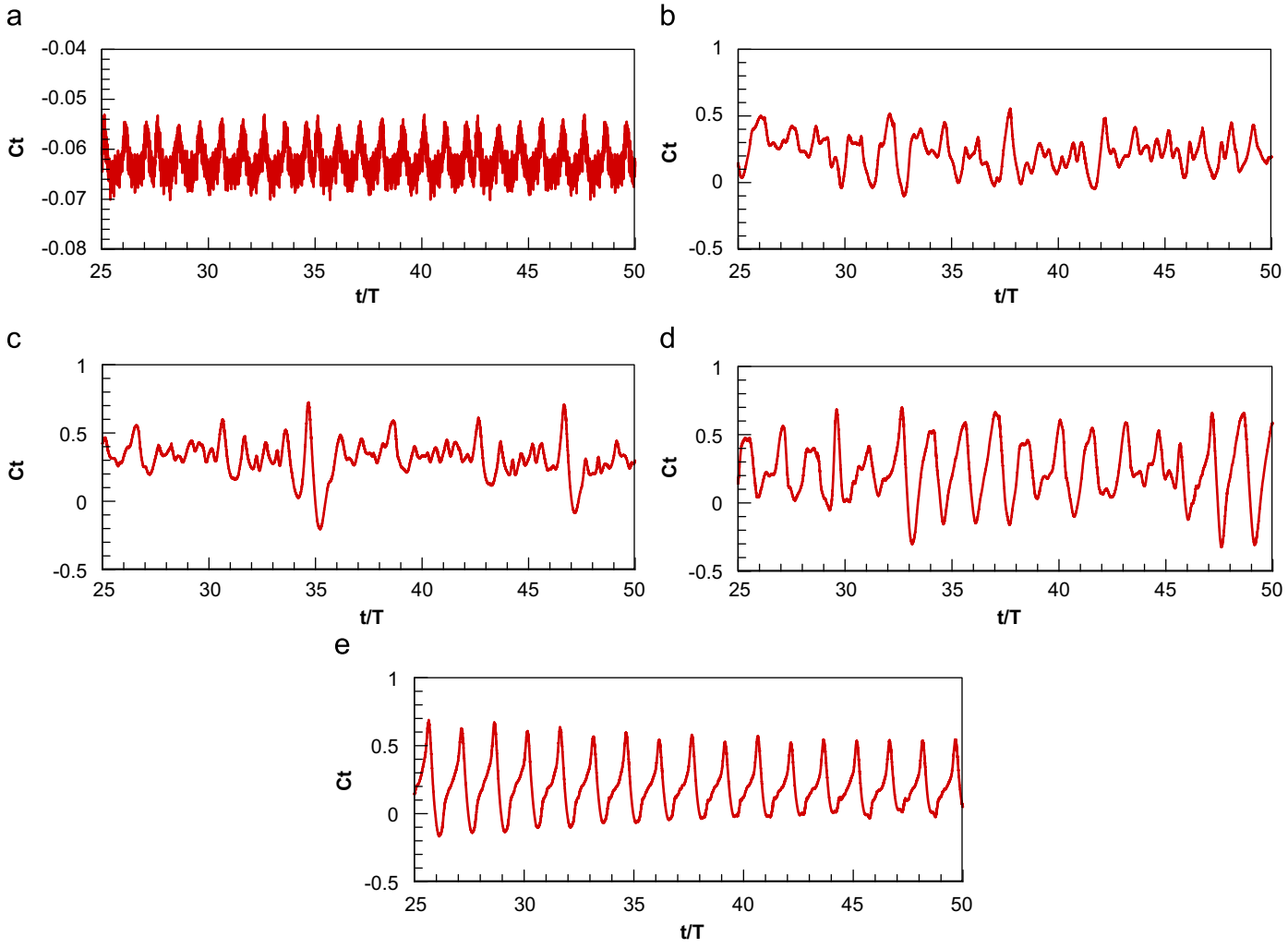

Fig. 10. Instant foil thrust coefficient evolution within 25 sequential periods. T is the period of foil undulation motion at St=0.12 (a) $L/D=\infty$, (b) L/D=0.5, (c) L/D=1.0, (d) L/D=1.5, and (e) L/D=2.0.

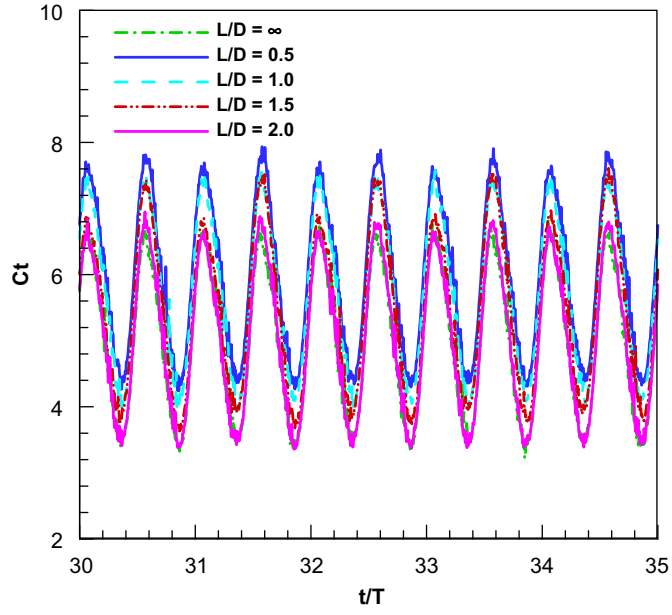

Fig. 11. Instant foil thrust coefficient evolution within 5 sequential periods. T is the period of foil undulation motion with St=1.18.

$St=1.18$ in Fig. 15, apparent difference in pressure distribution along the surface is shown for top and bottom walls. The trend is similar for all gap ratios including the single foil. On the foil top wall, pressure increases along the surface and reaches a maximum around $x/c=0.65$ then decreases until reaching the trailing edge. At the bottom wall, the pressure initially decreases along the surface, reaches a minimum pressure at $x/c=0.75$ then climbs up near the trailing edge. The peak pressure occurring at the back part of foil surface is consistent with the foil kinematic motion in which main body motion appears at the foil back half. The positive/negative peak pressure at this part definitely contributes to the thrust force in the forward direction considering the foil top convex and bottom concave shape at this instant time. Among all gap ratios, the peak value at $L/D=0.5$ is maximum and exhibits the best performance to thrust.

3.4. Combined cylinder and foil effect on cylinder drag and lift

From the above discussion, it is clear that, there are strong interactions between front D cylinder and backward foil in the wake of a cylinder. Such interactions not only affect the foil thrust force but also have impact on the cylinder drag force and lift coefficient. In this section, we discuss the foil effect on the cylinder hydrodynamic performance by exploring the cylinder time-mean, instantaneous drag coefficient, lift coefficient history and vorticity contours.

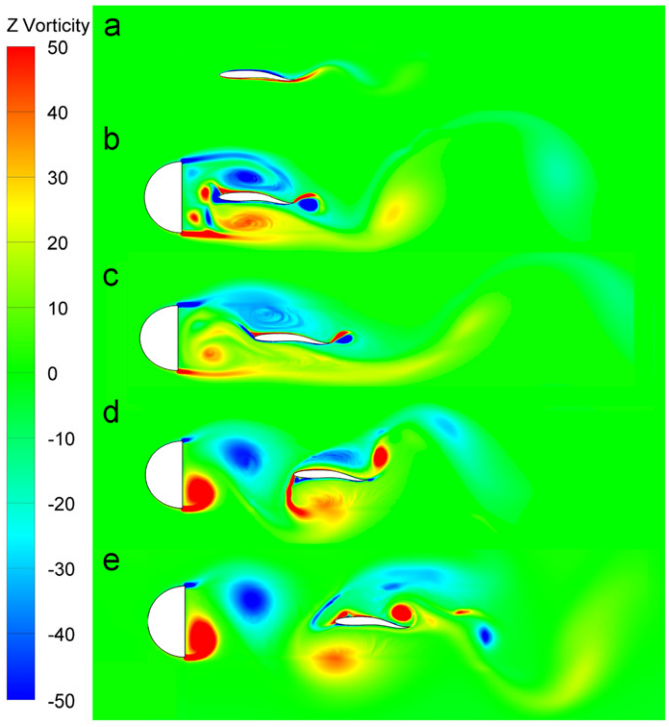

Fig. 12. Snapshot of vorticity contour at $t/T=0$ instant with frequency of $St=0.12$. (a) $L/D=\infty$, (b) $L/D=0.5$, (c) $L/D=1.0$, (d) $L/D=1.5$, and (e) $L/D=2.0$.

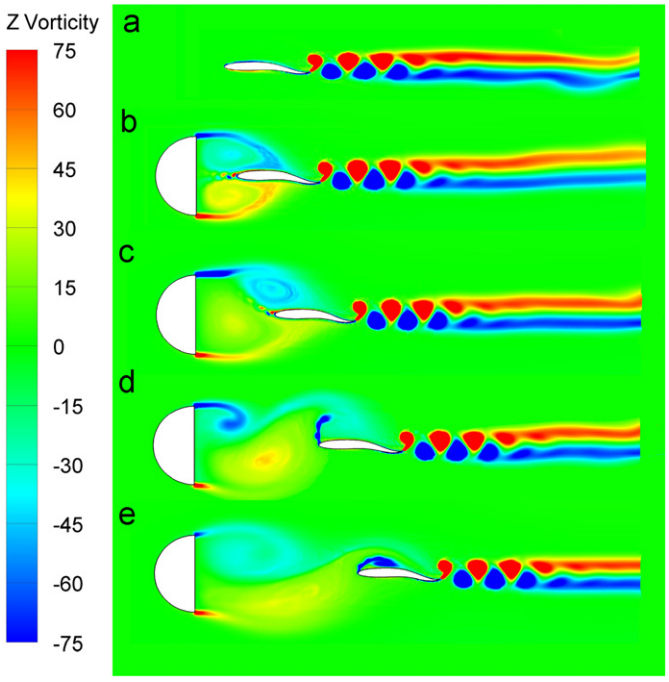

Fig. 13. Snapshot of vorticity contour at $t/T=0$ instant with frequency of $St=0.18$. (a) $L/D=\infty$, (b) $L/D=0.5$(c) $L/D=1.0$, (d) $L/D=1.5$, and (e) $L/D=2.0$

3.4.1. *Instant force characteristics*

Our computational results found that, the influence of undulating foil on the cylinder C_d and C_i are reflected by two folds, i.e. the vortex shedding frequency is manipulated as well as the time-mean drag. This is strongly relevant to the gap ratio and foil undulation frequency. The evolution of instant drag coefficient

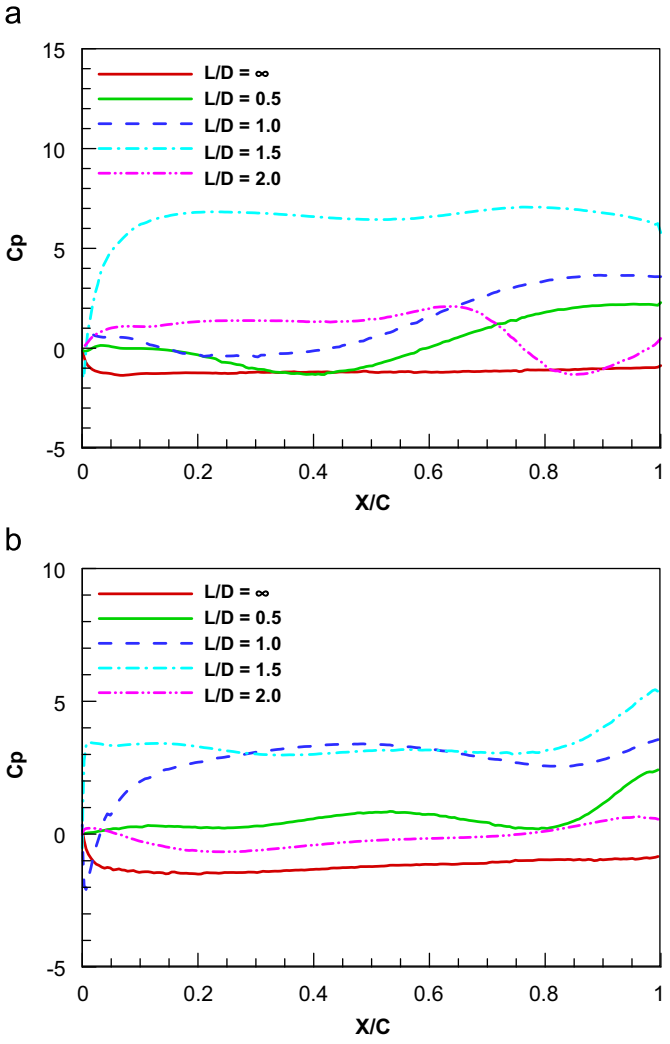

Fig. 14. Foil surface pressure distribution at 1/5T instant with $St=0.12$. (a) Top wall and (b) bottom wall.

and lift coefficient amplitude is shown in Figs. 16 and 17 for $St=0.12$ and 1.18, respectively.

At low frequency, such as $St=0.12$, with large gap ratios like $L/D=1.5$ and 2.0, the cylinder vortex shedding frequency is not affected by the insertion of foil as clearly seen from both instant C_d and C_i curves in Fig. 16. The frequency magnitude is the same as the cylinder alone but with the phase difference. As clearly revealed from the vorticity contours in Fig. 12(d) and (e), a pair of Von Kaman vortices is shedding form the top and bottom side of the cylinder in between the cylinder and the foil. Amplitude of C_d with large gap ratios, such as $L/D=1.5$ and 2.0 are larger than that of small gap ratios.

With close arrangement of foil and cylinder, such as $L/D=0.5$ and 1.0, the single dominant frequency does not appear, indicating the breakdown of cylinder vortex shedding in the wake caused by the strong foil interruption on the cylinder wake. The gap ratio effect on the lift coefficient history is similar to the drag behaviour. Although the time-mean lift coefficient is always zero, the amplitude of instant C_l decreases with $L/D=0.5$ and 1.0 compared to a cylinder alone and then increases with L/D.

At high foil undulation frequencies like $St=1.18$ in Fig. 17, the effect of gap ratio on C_d and C_l history is entirely different from that of low frequencies. At small gap ratios like $L/D=0.5$ and 1.0, the C_d curve presents one dominant frequency distinguishing from single cylinder vortex shedding frequency. Definitely, this indicates

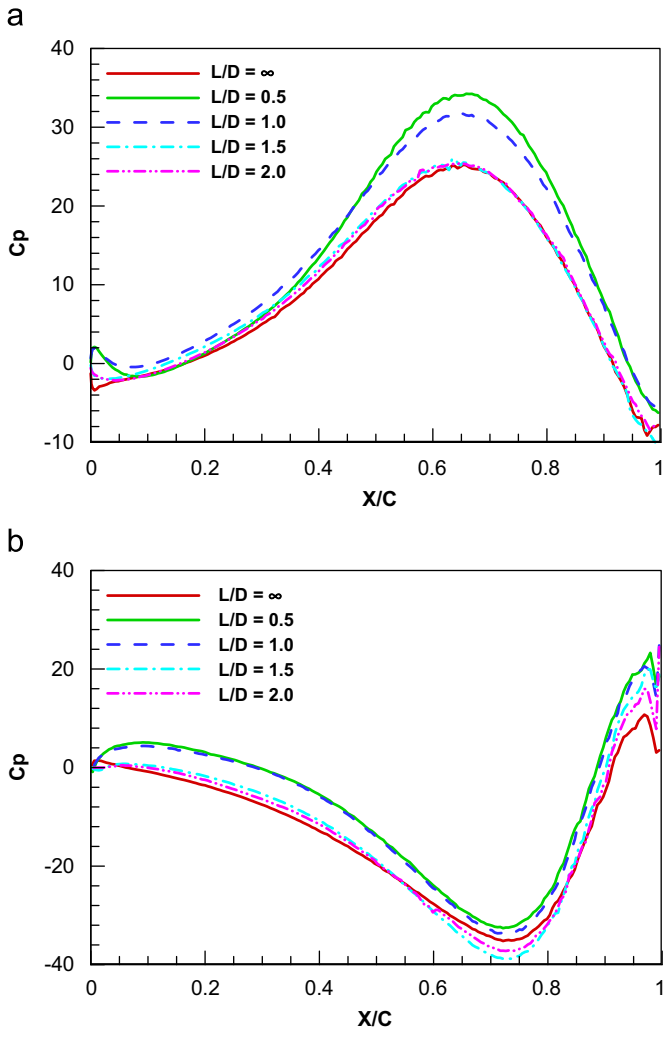

Fig. 15. Foil surface pressure distribution at 1/5T instant ith St=1.18. (a) Top wall and (b) bottom wall.

altered cylinder wake by the downstream foil undulating at such a high frequency. However, when L/D increases to 1.5 and 2.0, we can see that C_d curve varies less and less with time evolution. Detailed examination on the vorticity contour in Fig. 13(d) and (e) shows that the cylinder wake vortex stretches in the downstream with a weakened strength compared to single cylinder case.

3.4.2. Time-mean cylinder drag and lift amplitude

The gap spacing effect on the time-average cylinder drag coefficient and instant lift amplitude are shown in Figs. 18 and 19, respectively. The impact of foil on the cylinder depends very much on the gap spacing and frequency. At low frequencies like St=0.12 and 0.23, when the foil is imposed close to the front cylinder within a certain distance (L/D=0.5 and 1.0), C_d apparently decreases compared to when the foil is absent. Beyond this distance, the cylinder drag coefficient increases significantly with gap spacing, particularly at distance of L/D=2.0. However, at higher frequencies as St=1.18 and 1.76, increasing gap ratio leads to the profound drag reduction except when the foil is very close to the cylinder as L/D=0.5.

From Fig. 17 for the cylinder lift coefficient amplitude plot, it can be seen that, with insertion of undulation foil, C_l amplitude is increased with large gap ratios for high frequencies. The maximum increment can reach as high as eight times that of a single cylinder at L/D=0.5, indicating the dramatic increase of instant

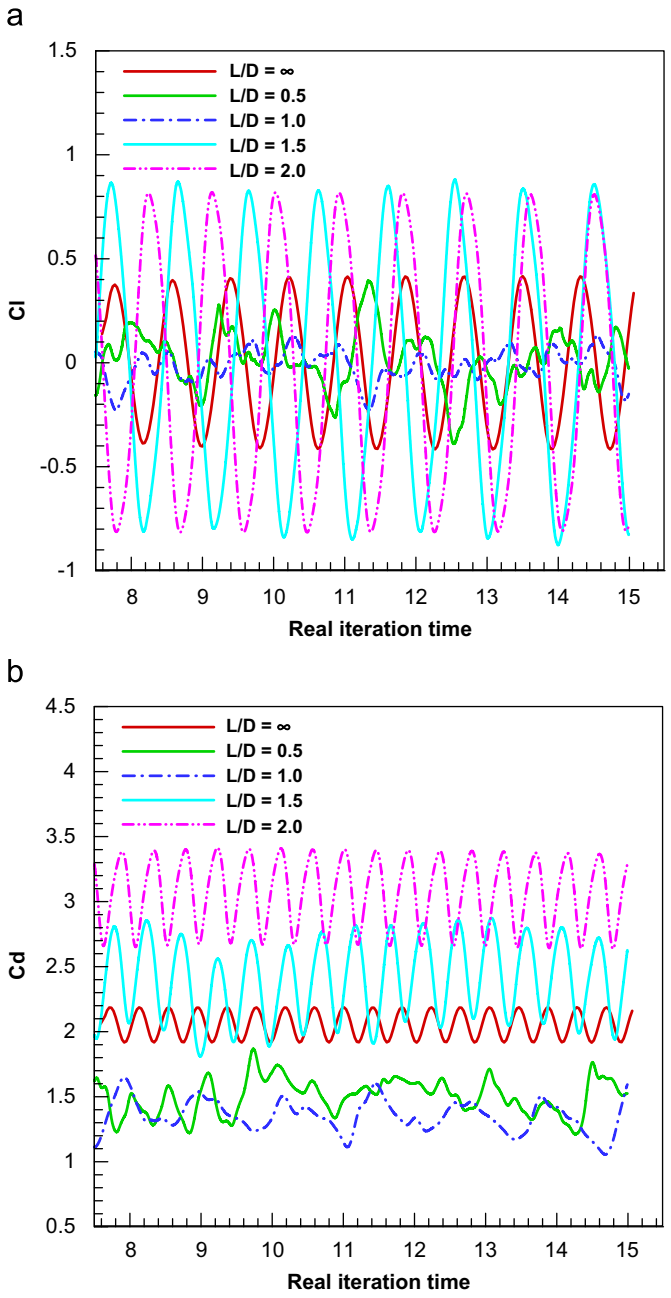

Fig. 16. Evolution of instant cylinder drag coefficient and amplitude of lift coefficient at St=0.12. (a) lift coefficient and (b) drag coefficient.

force in y-direction caused by the downstream high frequency undulation foil. At low frequencies, a minor decreased C_l amplitude is seen for L/D=0.5 and 1.0.

3.4.3. Cylinder wake structure

The mechanism of drag reduction/increase with undulation foil can be explained with the aid of comparison of cylinder wake vorticity contours for two particular cases of L/D=0.5 and 2.0 at St=0.12 and 1.18 to the single cylinder situation. It is well known that, the fundamental mechanism for cylinder drag reduction, via vortex control devices such as splitter devices, is achieved by delaying or breaking the Kaman vortex shedding in the cylinder wake. Similar mechanism is observed here with insertion of undulation foil. Clearly seen, for two drag reduction cases at frequencies of St=0.12 and 1.18, the cylinder vortex shedding, which is well built up in the cylinder alone case (as shown in Fig. 7(b)), is not developed.

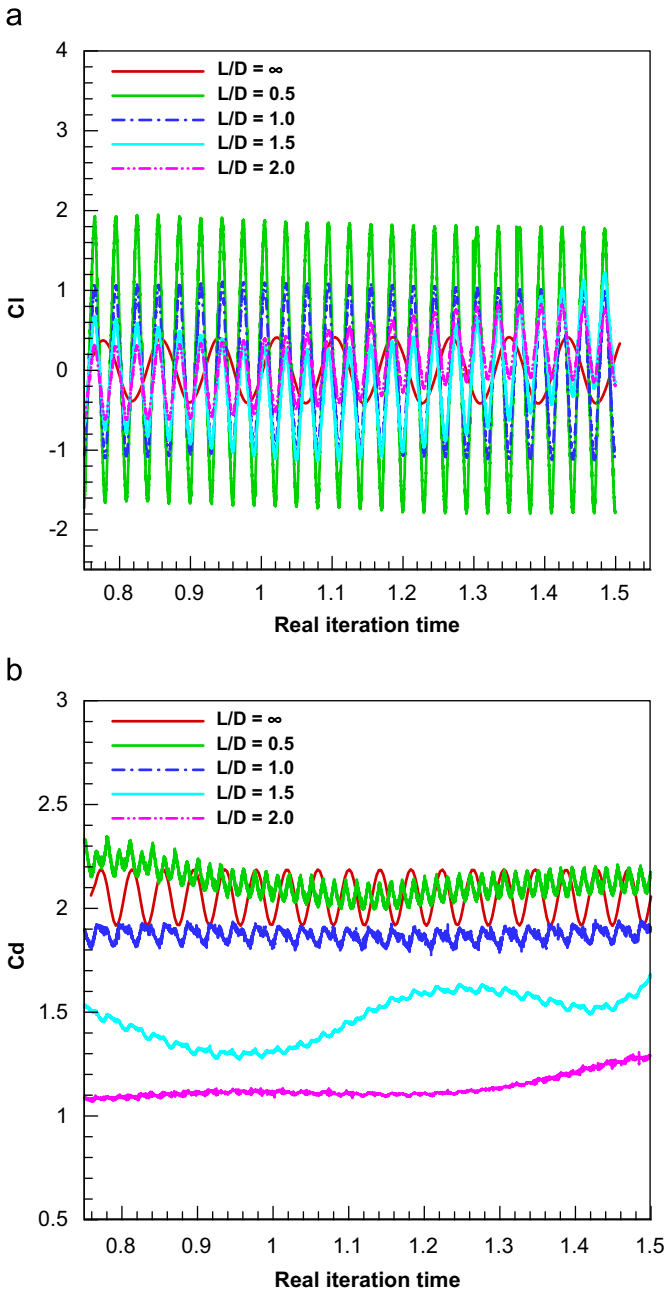

Fig. 17. Evolution of instant thrust/drag coefficient for foil and cylinder St=1.18. (a) Lift coefficient and (b) drag coefficient.

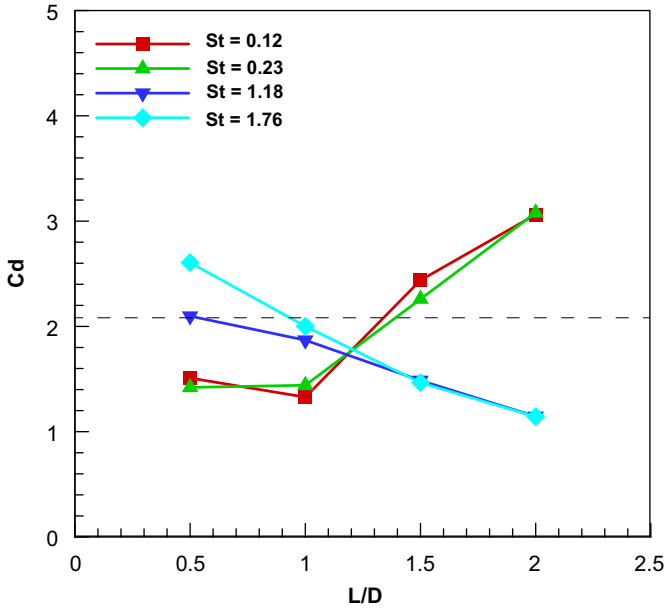

Fig. 18. Time-mean drag coefficient of cylinder variation with L/D (dashed line represents the drag coefficient of a cylinder alone).

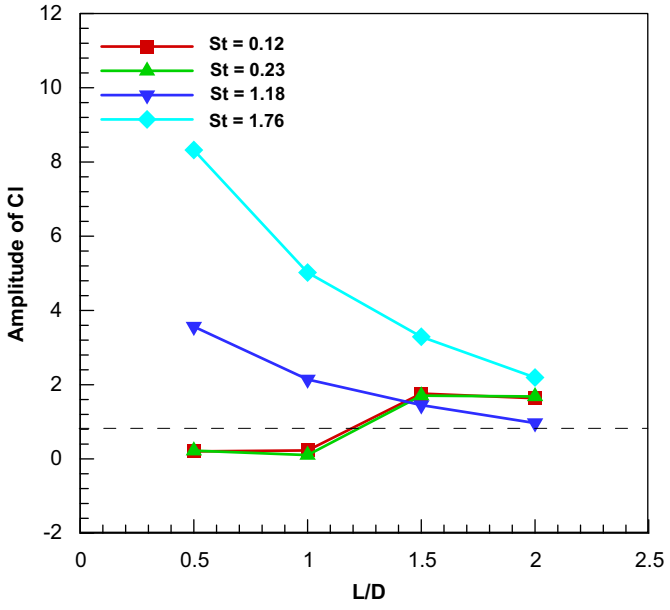

Fig. 19. Cylinder instant amplitude variation with L/D (dashed line represents the corresponding value of a cylinder alone).

Instead, they are either broken by the penetration of foil in the wake at low St=0.12 (Fig. 12(b)) or stretch in the stream-wise direction with foil at high St=1.18 (Fig. 13(e)) located further downstream. However, for the drag-increase cases such as St=0.12 and L/D=2.0, the vortex shedding structure is enhanced by the downstream foil as displayed in Fig. 12(e) compared to Fig. 7(b) for a single cylinder.

4. Conclusions

A numerical investigation on the interaction between undulation foil and upstream D-section cylinder is performed. The computation encompasses a wide range of frequency (St) and gap ratios (L/D). For the impact on the foil, it is found that, the thrust coefficient (C_t) with the appearance of cylinder is always larger than that of a cylinder absence for all undulation frequencies and gap ratios tested. A thrust coefficient, as high as eleven times that of the single foil, is achievable at low frequency. The reversed Kaman vortex street in the foil wake is enhanced by the presence of upstream cylinder.

However, the effects of undulating foil on the cylinder drag force and lift amplitude considerably rely on the gap ratio as well as undulation frequency.

For low frequency which is closer to the inherent cylinder vortex shedding frequency (St=0.25), the effect of the foil on the drag and lift amplitude reduction is significant when the foil is closer to cylinder ($L/D \leq 1.0$). By increasing gap ratio, the cylinder drag force and lift amplitude increase. For high frequencies, except for very close situation (L/D=0.5), the cylinder drag

coefficient considerably decreases with insertion of foil. However, lift amplitude is always larger than its counterpart in a single cylinder case. The distinctive difference is caused by the change in cylinder wake including the vortex shedding formation, size and strength with the insertion of undulation foil.

Acknowledgements

The second author would like to thank State Administration of Foreign Experts Affairs of China (Grant No. B07019) and Fundamental Research Foundation of Harbin Engineering University in China (Grant No. HEUFT08016) for providing her with financial support during the course of this research.

References

Breder, C.M., 1965. Vortices and fish schools. Zoologica 50, 97–114.
Beal, D.N., Hover, F.S., Triantafyllou, M.S., Liao, J.C., Lauder, G.V., 2006. Passive propulsion in vortex wakes. Journal of Fluid Mechanics 549, 385–402.
Choi, H., Jeon, W.P., Kim, J., 2008. Control of flow over a bluff body. Annual Review of Fluid Mechanics. 40, 113–139.
Eldredge, J.D., Pisani, D., 2008. Passive locomotion of a simple articulated fish-like system in the wake of an obstacle. Journal of Fluid Mechanics 607, 279–288.
Flanagan, P.J., 2004, Unsteady Navier–stokes simulation of rainbow trout swimming hydrodynamics, MSc. thesis, Washington State University, Department of Civil and Environmental Engineering.
Gopalkrishnan, R., Triantafyllou, M.S., Triantafyllou, G.S., Barrett, D., 1994. Active vorticity control in a shear flow using a flapping foil. Journal of Fluid Mechanics. 274, 1–21.
Herskin, J., Steffensen, J.F., 1998. Energy savings in sea bass swimming in a school: measurements of tail beat frequency and oxygen consumption at different swimming speeds. Journal of Fish Biology 53, 366–376.
Hinch, S.G., Rand, P.S., 2000. Optimal swimming speeds and forward-assisted propulsion: energy-conserving behaviours of upriver-migrating adult salmon. Canadian Journal of Fisheries Aquatic Sciences 57, 2470–2478.
Hwang, J.Y., Yang, K.S., Sun, S.H., 2003. Reduction of flow-induced forces on circular cylinder using a detached splitter plate. Physics of Fluids 15, 2433–2436.
Kwon, K., Choi, H., 1996. Control of laminar vortex shedding behind a circular cylinder using splitter plates. Physics of Fluids 8, 479–486.
Liao, J.C., Beal, D.N., Lauder, G.V., Triantafyllou, M.S., 2003a. Fish exploiting vortices decrease muscle activity. Science 302, 1566–1569.
Liao, J.C., Beal, D.N., Lauder, G.V., Triantafyllou, M.S., 2003b. The Karman gait: novel kinematics of rainbow trout swimming in a vortex street. Journal of Experimental Biology 206, 1059–1073.
Liao, Q., Dong, G.J., Lu, X.Y., 2004. Vortex formation and force characteristics of a foil in the wake of a circular cylinder. Journal of Fluids and Structures 19, 491–510.
Liao, J.C., 2007. A review of fish swimming mechanics and behaviour in altered flows. Philosophy of Transaction Royal Society B 362, 1973–1993.
Streitline, K., Triantafyllou, G.S., Triantafyllou, M.S., 1996. Efficient foil propulsion through vortex control. The American Institute of Aeronautics and Astronautics Journal 34, 2315–2319.
Strykowski, P.J., Sreenivasan, K.R., 1990. On the formation and suppression of vortex 'shedding' at low Reynolds numbers. Journal of Fluid Mechanics 218, 71–107.
Weihs, D., 1973. Hydromechanics of fish schooling. Nature 241, 290–291.
Webb, P.W., 1998. Entrainment by river chub Nocomis micropogon and smallmouth bass *Micropterus dolomieu* on cylinders. Journal of Experimental Biology 201, 2403–2412.
Zdravkovich, M.M., 1981. Review and classification of various aerodynamic and hydrodynamic means for suppressing vortex shedding. Journal of Wind Engineering and Industrial Aerodynamics 7, 145–189.